SACLANTCEN REPORT
serial no.: SR-165

SACLANT UNDERSEA RESEARCH CENTRE

REPORT

Satellite measurements of sea-surface temperature: Some consequences of variability on validation and applications

P.J. Minnett

July 1990

Page count for SR-165
(excluding covers)

Pages	Total
i–vi	6
1–37	37
	43

SACLANT Undersea Research Centre
Viale San Bartolomeo 400
19026 San Bartolomeo (SP), Italy

tel: 0187 540 111
fax: 0187 560 770
telex: 271148 SACENT I

NORTH ATLANTIC TREATY ORGANIZATION

SACLANTCEN SR-165

Satellite measurements of sea-surface temperature:

Some consequences of variability on validation and applications

P.J. Minnett

The content of this document pertains to work performed under Project 23 of the SACLANTCEN Programme of Work. The document has been approved for release by The Director, SACLANTCEN.

Peter C. Wille
Director

intentionally blank page

Satellite measurements of sea-surface temperature:

Some consequences of variability on validation and applications

P.J. Minnett

Executive Summary: Imaging radiometers on earth observation spacecraft offer the only feasible method of obtaining large-scale measurements of the sea-surface on a routine basis. Also the satellite data can be gathered from areas where it may be difficult for surface ships to operate. The accuracy of the satellite SST (sea-surface temperature) measurements is usually determined by comparing the satellite data with those derived from in situ sensors on, for example, drifting buoys. Largely because of the presence of clouds it is difficult to obtain an adequate number of comparisons in which the satellite and in situ measurements are simultaneous and collocated. Consequently it is necessary to relax this condition and allow comparisons to be made between measurements separated in space and/or in time. But this introduces errors into the comparison because of changes, both spatial and temporal, in the SST. It is the purpose of this study to determine the maximum tolerable temporal and spatial separations between the two measurements.

The analysis, presented here, of SST data from various sources – drifting buoys, satellite images and a research vessel – in the southern Norwegian Sea, shows that comparisons between satellite and in situ data must be restricted to measurements separated by less than about 10 km and 2 h. This is much more stringent condition than is usually applied in published comparisons, and implies that the satellite SST values could be considerably more accurate than the demonstrated level of 0.5 to 1 K.

A similar analysis is presented for the application of SST measurements in ocean modelling. It is shown that the SST measurements may still contribute meaningful information to a model even if they are displaced by up to about 20 km from a grid point and about 6 h from a time step. Given the usual time step of upper ocean models is about 1–2 h, the temporal constraint can be met easily, but the spatial constraint is stricter than that usually currently applied.

This report is of continuing work in Project 23 concerned with the quantitative determination of oceanographic variables from satellite measurements, and follows on from SR-137 in which theoretical accuracies of SST determination were derived.

intentionally blank page

SACLANTCEN SR-165

Satellite measurements of sea-surface temperature:

Some consequences of variability on validation and applications

P.J. Minnett

Abstract: Sea-surface temperature (SST) measurements from both spaceborne and in situ sensors are analysed to determine likely temperature differences that can arise between two measurements separated in space and time. This has implications both for satellite data validation, where an in situ measurement is compared with a remotely-sensed one, and for the use of SST measurements in numerical upper-ocean models, where an SST value is ascribed to, or compared with one from a nearby grid-point at the closest time-step. It is shown that spatial separations of $\sim$ 10 km and time intervals of $\sim$ 2 h can introduce rms differences of 0.2 K into the error budget of a satellite validation data set, which is an upper limit for the validation of current infrared radiometers. The length and time scales at which the autocorrelation functions decay to 0.5 are used as a criterion for the meaningful use of SST data with ocean models, and these are found to be $\sim$ 10–20 km and $\sim$ 6 h. This time constraint is not very severe, but the spatial constraint poses a significant sampling problem. On these length scales there appears to be no spatial anisotropy with respect to the dominant surface current flow direction, but there is some slight evidence that length scales are somewhat longer in daytime during the summer.

Keywords: data assimilation ○ ocean models ○ remote sensing ○ sea-surface temperature ○ validation

Contents

Acknowledgement: Tilde Pedenovi and Elvio Nacini assisted with the processing of the buoy and AVHRR data. Discussions with Dr. J. Ianiello (SPG) on the information content of the data sets were useful, and the co-operation of the master and crew of the HNLMS *Tydeman*, and Dr. T.S. Hopkins, Chief Scientist for the cruise GIN Sea '86, are acknowledged.

1 Introduction

While the images from the infrared channels of satellite scanning radiometers, such as the advanced very high resolution radiometer (AVHRR), provide a wealth of information about the positions and shapes of the surface expressions of thermal fronts, and about surface kinematics, the main scientific impact of these data is in the provision of accurate measurements of sea-surface temperature (SST). This potential has not yet been fully realised, partly because of the difficulty in assessing the accuracy of the AVHRR SST retrievals. As with all physical measurements, the utility of satellite SST fields is determined and restricted by their absolute accuracy and by confidence in the estimate of residual errors. For some applications relatively poor absolute accuracy but high relative accuracy is acceptable, while for others, such as climate research, high absolute accuracy of $< \pm 0.3$ K is required (Harries et al., 1983; Webster and Fieux, 1984).

The processes involved in deriving maps of SST from raw brightness-temperature images are:

- the calibration of the satellite measurement, which is done using measurements of an on-board black-body calibration target;
- the removal of pixels contaminated by cloud radiances, which is done by comparing visible and infrared measurements, or examining the spatial characteristics of the measured fields;
- the correction of the effects of the intervening atmosphere, which is done by combining measurements from two or three infrared channels.

All of these operations are imprecise in that they require the use of assumptions and approximations, and thus contribute to the residual uncertainties in the derived SST. These uncertainties are usually quantified by comparing satellite derived SSTs with those from in situ sensors. This 'validation' procedure is in itself prone to uncertainties that contribute to the total inaccuracies attributed to the satellite measurements.

With the development of new satellite instruments, such as the along-track scanning radiometer (ATSR) on ERS-1 (Minnett, 1990a), the advanced medium resolution imaging radiometer (AMRIR) (Sparkman, 1989) and the moderate-resolution imaging spectrometer (MODIS) (US NASA, 1986), and with improved data processing algorithms, the SST fields derived from satellite measurements will continue to be-

come more accurate. Attendant on these improvements is the growing need to have confidence in the in situ data used for validation and in the validation procedure itself.

The comparison between SST measurements from spaceborne and in situ sensors is not confined to the validation of the satellite data; it is also used to derive the coefficients used in the SST retrieval algorithm (e.g. Strong and McClain, 1984), to assess anomalous effects, such as the injection of large amounts of volcanic aerosols into the atmosphere (e.g. Walton, 1985), and to generate hybrid data sets with measurements from other sources. Also, the inclusion of satellite-derived SST in numerical models of both the ocean and the atmosphere involves implicitly the same uncertainties as a comparison with in situ data, but in this case the in situ data points are the values of the modelled SST field at model grid points.

For several reasons, such as obscuration by cloud or an inopportune time sampling imposed by the satellite orbit, the satellite-derived SST may not be precisely simultaneous or collocated with the associated in situ measurement or model simulation. Thus an uncertainty arises through the temporal and spatial variability of the SST field, and this restricts the applicability of a particular SST measurement (in situ or spaceborne) to represent a value elsewhere, such as at a 'nearby' model grid point, or at another time, such as at a 'close' satellite overpass.

The work presented here is an attempt to determine the displacements in space and intervals in time that limit their contribution to the final uncertainties in the determination of the accuracy of the satellite SST retrievals to acceptable levels.

2

Error budget for satellite SST validation

Numerical simulations of the effects of the atmosphere on AVHRR measurements predict SST retrieval accuracies of $\sim$ 0.2–0.6 K when expressed as standard deviations about a mean error that is zero (Llewellyn-Jones et al., 1984; Minnett, 1986; Minnett, 1990b). These values include the effects of inherent instrument (detector) noise and residual errors due to atmospheric variability which is has a dependence on the atmospheric path length, i.e. the errors increase towards the edges of the image. These values are augmented by the uncertainties associated with the internal calibration procedure of the AVHRR, which is at best at the level of $\sim \pm 0.2$ K (Brown et al., 1985). In total, therefore, the accuracy of AVHRR SST retrievals should be in the range of ± 0.3 K to ± 0.7 K (Table 1), with the best accuracy being achieved by measurements through relatively dry atmospheres close to nadir, i.e. at the centre of the AVHRR image, which is through the shortest atmospheric path length.

There are several published reports in which the SST values derived from AVHRR measurements have been compared with individual high quality in situ measurements; usually the discrepancies found have mean values of $< \pm 0.5$ K and standard deviations of $\sim$ 0.4 K to $\sim$ 1 K (e.g. Bernstein, 1982; McClain et al., 1983; Llewellyn-Jones et al., 1984; Strong and McClain, 1984; Barton et al., 1989; Castagne et al., 1986; Schluessel et al., 1987; Le Borgne et al., 1988; McClain, 1989).

In general, it would appear that the theoretical accuracy of AVHRR SST retrievals has not been demonstrated by comparison with in situ measurements. But, of course, these figures include contributions from uncertainties in the in situ measurement and errors introduced by the method of comparison. Ideally the validating instrument should measure the same quantity as the spaceborne sensor, which requires the use of an infrared radiometer, such as described by Hepplewhite (1989), who estimates the accuracy of such an instrument as $\sim \pm 0.25$ K. Better accuracy can be achieved using in situ thermometers, such as those on free-drifting buoys, accurate to ± 0.1 K, or those of precision oceanographic instruments, which are accurate to $< \pm 0.01$ K. Unfortunately, the measurements of these highly accurate in situ thermometers may be decoupled from the true SST by near-surface temperature gradients. These are caused by heat loss to the atmosphere that giving rise to the so-called thermal 'skin effect', and the diurnal thermocline which occurs in situations of strong insolation and low wind speed. The skin effect generally lowers the SST with respect to the measurement at a depth greater than a few millimetres by a variable amount, up to many tenths of a Kelvin (Robinson et al., 1984), with 0.3 K being found to

Table 1 *Error budgets*

	Uncertainty/ Range (K)	Comments
*Theoretical accuracies**		
AVHRR calibration	± 0.2	Brown, Brown and Evans (1985)
Detector noise	± 0.02	Reduced from single pixel value by spatial averaging – 6×6 pixels
Residual atmospheric effects (split window, regional optimised algorithm)	$[\pm 0.2, \pm 0.6]$	Minnett (1989)
Total	$[\pm 0.3, \pm 0.7]$	
In situ thermometer		
Sensor		
buoy	± 0.1	
CTD	$< \pm 0.01$	
Skin effect	$[0.0, -0.5]$	Robinson, Wells and Charnock (1984), Hepplewhite (1989)
Diurnal thermocline	$[0.0, +1.5]$	Cornillon and Stramma (1985)
Total	$[-0.6, +1.6]$	
Sea-level radiometer		
Sensor	± 0.25	Hepplewhite (1989)
Total	± 0.25	
Lack of collocation and simultaneity		
Spatial gradients	$< \pm 0.2$	Necessary limit
Temporal changes	$< \pm 0.2$	Necessary limit

* Clear atmosphere.

be a representative value for the North Atlantic Ocean (Hepplewhite, 1989). The sunshine may warm the near-surface layer to a depth of several tens of centimetres or more by as much as 1 K, or exceptionally 2 K (Cornillon and Stramma, 1985), in conditions of low wind speed. The near-surface gradients, called the diurnal thermocline, are maximum in late afternoon and smallest around sunrise, after the night-time cooling and before the onset of daytime surface heating.

To avoid further uncertainties caused by the effects of residual cloud contamination[1], the validation measurements must be taken in conditions of very clear skies, which, since such conditions are favourable to the generation of a diurnal thermocline,

[1] Minnett et al. (1984) present some evidence to show that residual effects in areas where cloud cover is 40% or more are a few tenths of a kelvin, although this is very dependent on the cloud detection procedure used and the cloud types present.

implies using early morning data. Even with this restriction the amount of AVHRR data that can be used in a validation exercise is very large. The number of validation data points is limited in reality by the availability of the in situ measurements.

In an ideal situation the in situ measurement should be made at precisely the same time and place as the satellite measurement. For a variety of reasons this is rarely the case. The biggest single cause of the loss of contemporaneous and collocated data is the presence of clouds obscuring the position of the in situ measurement when mapped into the satellite image. In reality, to obtain a reasonable number of pairs of in situ and satellite measurements it is necessary to relax the precise requirement of exact coincidence and permit the comparison to be made between data points separated in space and time. Since the SST field is highly variable, the relaxation of precise coincidence introduces errors into the comparison, and these will depend on what is deemed to be acceptable displacements or time intervals between the satellite measurement and the corresponding in situ measurement. For the purposes of this study, contributions to the error budget (Table 1) of up to 0.2 K from the lack of spatial or temporal coincidence are taken as the maximum tolerable values.

3

Methodology

A complete description of the variability of SST requires comprehensive measurements on all spatial scales of interest over the time intervals of interest, which is of course not possible. Consequently, various data sources have been used, each to explore a particular facet of the SST variability. The spatial variations are investigated using sections extracted from cloud-free portions of infrared images from the AVHRR itself. Images taken from satellite overpasses during the day and night and from summer and winter seasons are used to investigate the possibility of systematic differences. The temporal evolution of the SST field is described using data from two free-drifting buoys that transmit their measurements via the ARGOS satellite data collection and location system (DCLS). Finally, since, for satellite validation purposes at least, research ships are likely to be the main source of high qualify SST measurements, data from a cruise of the *Tydeman* (NL) are used to examine the mixture of temporal and spatial variability as perceived during an oceanographic research cruise.

All data were taken in the area of the southern Norwegian Sea as part of the Centre's GIN Sea programme.

3.1. ANALYSIS TECHNIQUE

The autocorrelation function (a.c.f.) of a variable is the appropriate measure of the amount of common variation between the variable sampled twice, separated by a given time interval, if the variable is expressed as a time series or by a given displacement, for a spatial series. The a.c.f. $R(\Delta)$ at lag Δ (equal to j times the sampling interval) of a discretely sampled variable T may be estimated by

$$R(\Delta) = \frac{\sum_{k=1}^{N-j} \left[(T_k - \bar{T}_k)(T_{k+j} - \bar{T}_{k+j})\right]}{\left[\sum_{k=1}^{N-j}(T_k - \bar{T}_k)^2\right]^{1/2} \left[\sum_{k=1}^{N-j}(T_{k+j} - \bar{T}_{k+j})\right]^{1/2}}, \tag{1}$$

where the overbar denotes a mean value. For small lags (i.e. much less than the length of the time or spatial series) and for stationary time series or homogeneous spatial series, the a.c.f. can be well approximated by

$$R(\Delta) = \frac{\overline{(T_k - \bar{T})(T_{k+j} - \bar{T})}}{\sigma^2}, \tag{2}$$

where σ^2 is the variance of the time/spatial series and $\bar{T}$ is its mean value.

The root-mean-square (rms) difference δ between measurements separated by Δ is related to the value of the a.c.f. at lag Δ by

$$\delta^2 = 2\sigma^2(1 - R(\Delta)), \tag{3}$$

i.e.

$$R(\Delta) = 1 - \delta^2/2\sigma^2. \tag{4}$$

Thus, for data sets with larger variances the lag at which the a.c.f. needs to decay to reach given rms differences is smaller than for data sets with small variance, and if the required rms difference is equal to the standard deviation of the data set, the appropriate lag is that for which the a.c.f. has reached the value of 0.5.

Expression (4) was used with each of the data sets from the drifting buoys and from the AVHRR images (see Subsects. 3.2 and 3.3). In each case a linear least-squares trend was removed from the data before calculating the a.c.f. of the residual fluctuations.

For the SST measurements taken from the research ship *Tydeman* (see Subsect. 3.4), neither the time-lagged or space-lagged a.c.f. is an appropriate function since the data contain both temporal and spatial changes. Consequently, a simple statistical analysis was performed on data segments of varying lengths.

3.2. DRIFTING BUOY DATA

During the second leg of the GIN Sea '87-1 cruise of the research vessel *Maria Paolina G.* (I), two air-sea interaction drifting (ASID) buoys were launched in the Faeroes–Shetland Channel. Buoy 4126 was deployed on 1 June 1987 (day 152) at 61°19′N, 3°07′W, and buoy 4125 on 2 June 1987 (day 153) at 62°58′N, 2°33′W. Their subsequent trajectories are shown in Fig. 1. These buoys, designed and constructed by the Polar Research Laboratory, USA, consist of a small surface spar buoy with a flotation collar in the form of an inverted cone. A small meteorological measurement package is mounted on the buoy which also supports a 300 m long thermistor chain. Sea-surface temperature is measured by a thermistor inside the hull of the buoy, at a depth of $\sim$ 1 m. The data from all the buoy sensors were sampled each minute and block averaged over 8 samples and broadcast to the DCLS (data collection and location system) on the NOAA (National Oceanic and Atmospheric Administration, USA) series of polar-orbiting weather satellites. The positions of the buoys at the time of the data reception are added to the data stream. Because the telemetry to the satellite functions only when the satellite is above the buoy's horizon, which happens for intervals of up to $\sim$ 15 min several times each day (at these latitudes this may be up to 12 times per day, but not uniformly distributed around the clock), the

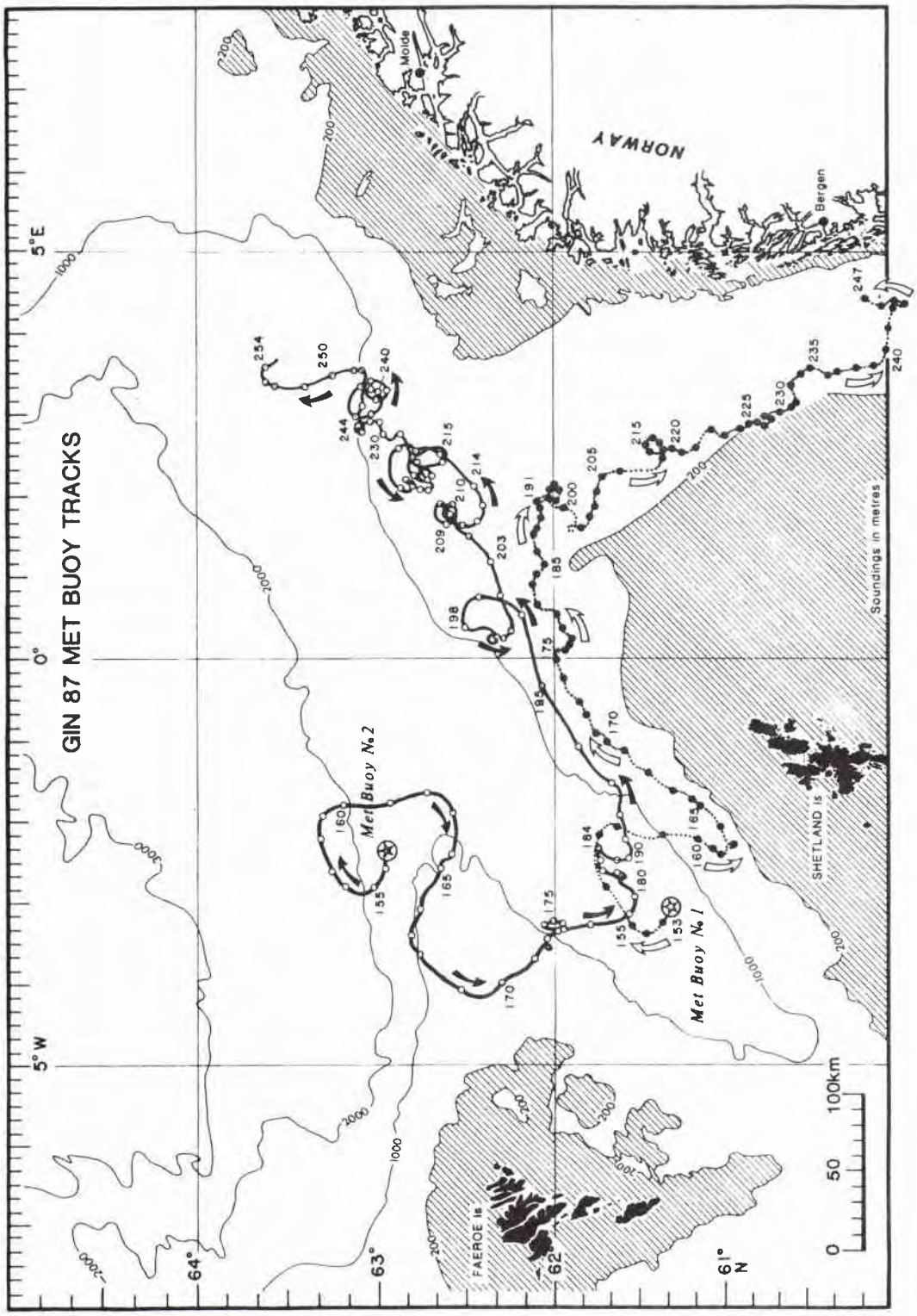

Figure 1 *Trajectories of two air-sea interaction drifting (ASID) buoys in the southern Norwegian Sea, during the summer of 1987. Tick marks on the trajectories show the position at midnight each day. Met Buoy 1: Buoy 4126; Met Buoy 2: Buoy 4125.*

Table 2 *Statistics of SST measurements from ASID Buoys (1987)*

Date/time (start)	Date/time (end)	N	$\overline{SST}$ (°C)	SST′ (K)	Trend (mK/d)	σ^2 (K^2)	$R(\tau_{0.2\,K})$*	$\tau_{0.2\,K}$ (h)	$\tau_{1/2}$** (h)
Buoy 4125									
3 Jun 02:30	31 Sep 19:30	2154	11.264	1.534	47.8	0.822	0.970	6.1	144
						(0.327)	*(0.813)*	*(19)*	*(57)*
Buoy 4126									
7 Jun 12:30	31 Sep 19:30	2192	12.001	1.699	58.9	0.467	0.908	2.5	61
						(0.390)	*(0.869)*	*(3.8)*	*(32)*

Values in parentheses refer the residuals after a least-squares quadratic function has been removed from each time series.

* $R(\tau_{0.2\,K})$: value of the time-lagged autocorrelation function which gives rms differences of 0.2 K between samples separated by $\tau_{0.2\,K}$ h.

** $\tau_{1/2}$: time lag at which the autocorrelation function has the value 0.5.

Table 3a *Buoy 4125: 10 days data segments*

Start day	N	$\overline{SST}$ (°C)	SST′ (K)	Trend (K/h)	σ^2 (K^2)	$R(\tau_{0.2\,K})$	$\tau_{0.2\,K}$ (h)	$\tau_{1/2}$ (h)
153	214	8.763	0.275	−0.101	0.089	−1.548	–	5.8
163	240	8.946	0.443	0.031	0.435	0.894	3.6	16.0
173	240	10.228	0.273	0.056	0.220	0.586	4.2	5.0
183	240	11.098	0.347	0.094	0.217	0.576	6.3	7.2
193	240	12.300	0.827	0.259	0.349	0.835	3.0	7.0
203	240	12.534	0.437	−0.062	0.400	0.875	8.1	25.5
213	240	12.672	0.267	0.050	0.224	0.602	12.1	21.8
223	240	12.872	0.403	−0.099	0.283	0.750	6.5	13.2
233	240	11.669	0.265	−0.073	0.162	0.242	16.2	9.0

*Symbols are as in Table 2.

Table 3b *Buoy 4126: 10 days data segments*

Start day	N	$\overline{SST}$ (°C)	SST′ (K)	Trend (K/h)	σ^2 (K^2)	$R(\tau_{0.2\,K})$	$\tau_{0.2\,K}$ (h)	$\tau_{1/2}$ (h)
153	240	9.520	0.289	0.007	0.289	0.761	1.9	7.0
163	240	9.649	0.417	0.015	0.416	0.884	1.6	4.0
173	240	10.933	0.378	0.074	0.313	0.795	2.0	3.6
183	240	11.215	0.552	0.080	0.502	0.921	2.5	14.6
193	240	12.836	0.858	0.242	0.496	0.919	0.9	3.3
203	240	13.232	0.720	−0.101	0.660	0.954	1.4	20.3
213	240	12.903	0.529	0.043	0.516	0.925	1.3	8.2
223	240	13.878	0.337	−0.019	0.333	0.820	1.6	3.6
233	240	13.846	0.232	−0.008	0.232	0.627	2.4	3.4

*Symbols are as in Table 2.

SST time series from each buoy is quite irregular, consisting of a number of 'bursts' of data each day. Furthermore, the data contain a significant number of false values, presumably caused by transmission errors. The data processing involved replacing these false measurements, which were easily identified as 'spikes' in the time series, with linearly interpolated values and block-averaging the resultant time series over intervals of one hour. Hourly intervals in which no data were recorded were assigned linearly interpolated values from their neighbours.

The final time series are shown in Figs. 2a and 3a. Time-lagged autocorrelation functions (a.c.f.) were calculated for each time series, after the removal of a linear trend, and are shown in Figs. 2b and 3b. The statistics of each time series are given in Table 2, which also includes the properties of the residuals after the removal of quadratic trends. Each time series was then segmented into ten-day intervals and the a.c.f. calculated for each segment. The results are given in Tables 3a and 3b.

Table 4 *AVHRR images*

Date	Time[1]	Satellite	Revolution	Comments
16 Nov 1984	14:54	NOAA-7	17538	winter, daytime
16 Jun 1986	13:04	NOAA-9	7756	summer, daytime
21 Jun 1986	03:53	NOAA-9	7821	summer, night-time

* Infrared data were extracted from cloud-free parts of images of the southern Norwegian Sea.
[1] UTC.

3.3. AVHRR SECTIONS

Linear sections extracted from infrared images of the southern Norwegian Sea were used to determine the spatial variability of SST. To avoid the consequences of the amplification of noise resulting from a multi-channel atmospheric correction scheme, data taken from the calibrated brightness temperature images from AVHRR channel 4 (T_4) were used (see Appendix A). The results of failing to account for the effect of the intervening atmosphere are twofold: firstly, the absolute values of the brightness temperatures are different from the SST, usually a few degrees cooler – but that is of no consequence here; and secondly, the apparent surface temperature variability is attenuated by $\sim 10\%$ in our case. Thus, before applying expression (4) to the a.c.f., the variance of the T_4 sections was increased by 10%.

To investigate the possibility of diurnal or seasonal dependence on the character of the SST variability, three T_4 images were used (Table 4). The same sections were extracted from each image and, in an attempt to avoid any bias in the choice of sections towards areas of particularly high or low variability, these were defined by

the station grid of the research cruise of the *Tydeman* (NL) in 1986 (Hopkins, 1988). The sections do not necessarily follow the track of the ship during the cruise, but connect the positions of the oceanographic stations (Fig. 4), and thus form a grid in which some of the sections are along the direction of the Atlantic Inflow into the Norwegian Sea and others cut across it. (Note that these AVHRR data are not directly comparable to the measurements from the Tydeman because of the lack of simultaneity.) The labelling of the sections has no significance other than to identify them, and because of the different patterns of cloudiness in each image, the sections from different overpasses are not directly comparable. Indeed, many sections are absent from some images because of the problem of cloud cover and others have been divided into shorter segments when clouds have obscured part of them. The satellite images are shown in Figs. 5–7 and the sections are listed in Tables 5–7. Two sample temperature sections with their a.c.f. are shown in Figs. 8 and 9.

3.4. TYDEMAN GIN SEA '86 CRUISE DATA

The SST variability as perceived from a research ship was examined by studying SST measurements from a cruise of the *Tydeman* (NL) in the southern Norwegian Sea in June 1986. The *Tydeman* is equipped with a system of automatically recording meteorological and oceanographic variables, including SST. The data used here are one-minute samples taken when the vessel was travelling between oceanographic stations at speeds greater than 0.25 ms^{-1}, to ensure good flushing of the sensor. The available data, taken during a period of 22 days, were divided into segments of varying lengths (1, 5, 10, 20, 30, 40, 50 and 100 km) and the standard deviations of SST in each segment were calculated. The mean ($\pm$ one standard deviation) of these standard deviations are shown in Fig. 10 as a function of segment length. This gives a measure of the differences in SST between measurements separated by various displacements, and, naturally, larger values are associated with longer displacements.

Figure 2a *The SST time series measured at a depth of ca. 1 m from the drifting Buoy 4125. Tick-marks on the time axis are at midnight of each day.*

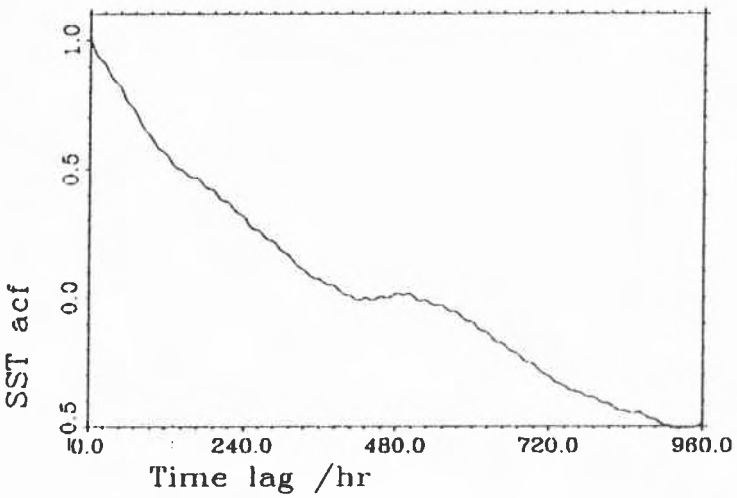

Figure 2b *The SST time series: time-lagged autocorrelation function.*

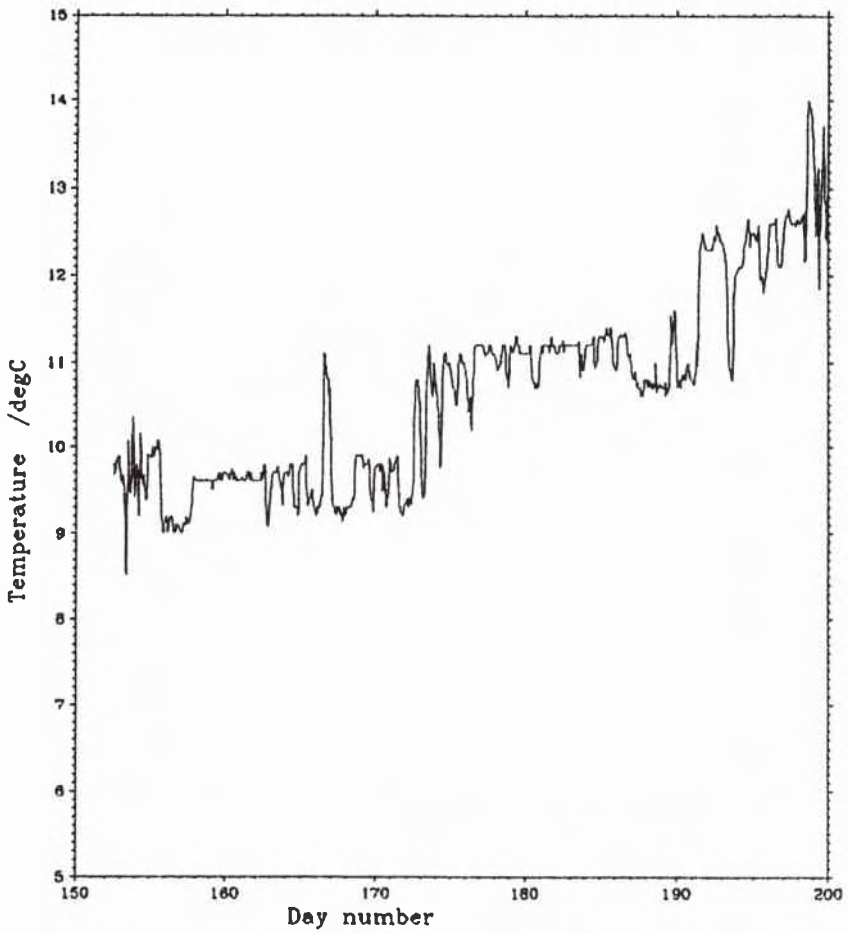

Figure 3a *The SST time series measured at a depth of ca. 1 m from the drifting Buoy 4126. Tick-marks on the time axis are at midnight of each day.*

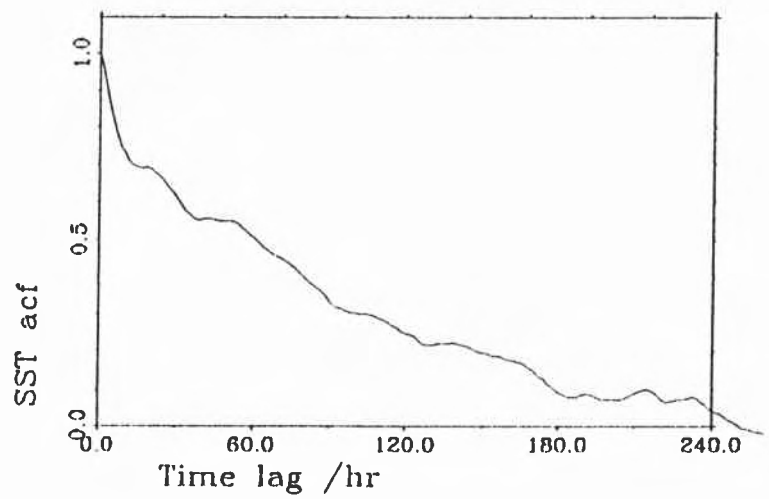

Figure 3b *The SST time series: time-lagged autocorrelation function.*

Table 5 *Statistics of T_4 sections from NOAA-7 AVHRR/2 - Revolution 17538 (16 November 1984 at 14:54 UTC)*

Sect.	N	Length (km)	$\overline{T_4}$ (°C)	T_4' (K)	Trend (mK/km)	σ^2 (K^2)	$R(\Delta_{0.2\,K})$*	$\Delta_{0.2\,K}$* (km)	$\Delta_{1/2}$* (km)
H	342	178	7.291	0.597	8.50	0.165	0.890	3.3	15.0
K	516	232	6.967	0.775	9.96	0.150	0.878	4.3	14.0
L	516	454	6.743	0.749	5.34	0.071	0.745	3.7	8.1
S	516	169	7.912	0.204	1.22	0.038	0.523	7.7	8.2
Xa	239	329	7.362	0.546	0.52	0.297	0.939	4.6	25.0
Xb	186	242	6.324	0.563	1.65	0.306	0.940	2.4	12.0
Ya	153	160	8.133	0.095	−0.32	0.009	−1.032	–	4.2
Yb	264	279	7.045	0.288	1.11	0.075	0.758	6.6	12.0
Za	213	368	7.722	0.354	3.00	0.018	−0.014	2.9	6.3
Zb	184	291	7.124	0.406	3.58	0.075	0.759	5.8	11.0

* Values are derived using variances of T_4 fluctuations increased by 10% to account for the effects of atmospheric transmission. Dashed entries indicate that the value of $R(\Delta_{0.2\,K})$ is not encountered. $R(\Delta_{0.2\,K})$ is the value of the autocorrelation function which gives rms differences of ±0.2 K between samples separated by $\Delta_{0.2\,K}$ km. $\Delta_{1/2}$ is the lag at which the autocorrelation function has the value 0.5.

Table 6 *Statistics of T_4 sections from NOAA-9 AVHRR/2 - Revolution 7756 (16 June 1986 at 13:04 UTC)*

Sect.	N	Length (km)	$\overline{T_4}$ (°C)	T_4' (K)	Trend (mK/km)	σ^2 (K^2)	$R(\Delta_{0.2\,K})$*	$\Delta_{0.2\,K}$* (km)	$\Delta_{1/2}$* (km)
A	516	90	7.289	0.476	17.84	0.012	−0.559	–	5.0
B	516	66	8.843	0.191	8.92	0.007	−1.517	–	3.5
C	516	133	8.697	0.359	7.30	0.047	0.614	1.6	2.7
Da	162	60	8.659	0.156	3.20	0.021	0.147	4.8	2.7
Db	259	100	8.541	0.192	5.73	0.009	−0.973	–	3.2
E	516	131	8.698	0.151	2.15	0.016	−0.127	3.4	6.6
F	492	218	8.812	0.202	2.42	0.018	−0.043	2.7	7.9
G	501	198	8.553	0.516	8.50	0.029	0.371	1.5	11.0
H	483	253	8.593	0.653	8.70	0.020	0.111	1.4	8.4
L	265	231	8.974	0.213	0.40	0.045	0.595	1.6	2.0
M	516	264	6.485	1.220	15.56	0.091	0.801	2.6	7.5
S	576	170	9.046	0.437	6.03	0.104	0.825	2.4	7.5
U	436	187	8.737	0.198	0.48	0.039	0.532	8.8	9.2
X	327	477	8.559	0.353	1.85	0.056	0.676	9.2	15.0
Y	363	447	8.650	0.250	0.23	0.062	0.707	1.5	31.0
Z	517	811	8.922	0.319	0.99	0.043	0.576	1.8	25.0

* Values are derived using variances of T_4 fluctuations increased by 10% to account for the effects of atmospheric transmission. Dashed entries indicate that the value of $R(\Delta_{0.2\,K})$ is not encountered. $R(\Delta_{0.2\,K})$ is the value of the autocorrelation function which gives rms differences of ±0.2 K between samples separated by $\Delta_{0.2\,K}$ km. $\Delta_{1/2}$ is the lag at which the autocorrelation function has the value 0.5.

Table 7 *Statistics of T_4 sections from NOAA-9 AVHRR/2 - Revolution 7821 (21 June 1986 at 03:53 UTC)*

Sect.	N	Length (km)	$\overline{T_4}$ (°C)	T_4' (K)	Trend (mK/km)	σ^2 (K^2)	$R(\Delta_{0.2\,K})$*	$\Delta_{0.2\,K}$* (km)	$\Delta_{1/2}$* (km)
F	492	218	8.182	0.217	−0.34	0.047	0.611	6.8	9.4
G	372	149	8.222	0.170	−2.61	0.016	−0.106	15.0	5.0
H	260	139	7.725	0.301	2.27	0.083	0.780	2.0	4.4
L	278	237	7.582	0.293	3.65	0.023	0.197	22.0	3.2
M	425	216	6.725	0.766	−11.52	0.067	0.727	3.1	6.1
S	213	70	7.672	0.209	−5.27	0.032	0.436	3.3	2.9
Xa	163	214	8.191	0.225	−0.63	0.049	0.632	7.2	10.0
Xb	145	192	7.747	0.207	−2.46	0.025	0.260	9.3	4.9
Ya	177	209	8.143	0.177	−0.53	0.031	0.410	6.5	5.5
Yb	122	145	7.740	0.356	0.68	0.127	0.856	0.8	2.4

* Values are derived using variances of T_4 fluctuations increased by 10% to account for the effects of atmospheric transmission. $R(\Delta_{0.2\,K})$ is the value of the autocorrelation function which gives rms differences of ±0.2 K between samples separated by $\Delta_{0.2\,K}$ km. $\Delta_{1/2}$ is the lag at which the autocorrelation function has the value 0.5.

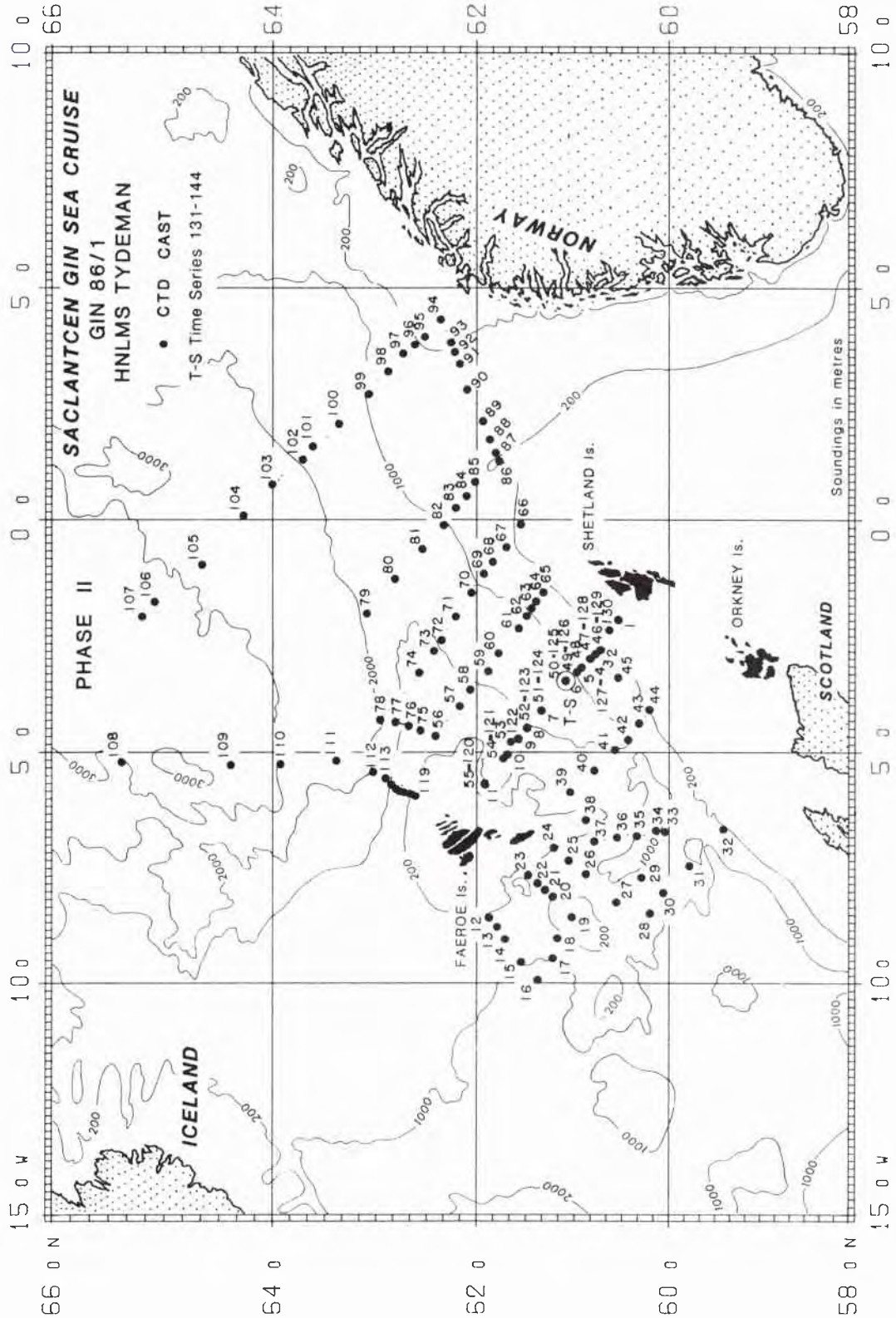

Figure 4 *Oceanographic stations occupied by the HNLMS Tydeman during the GIN Sea '86 cruise of June 1986. The data used here were collected during the transects between stations.*

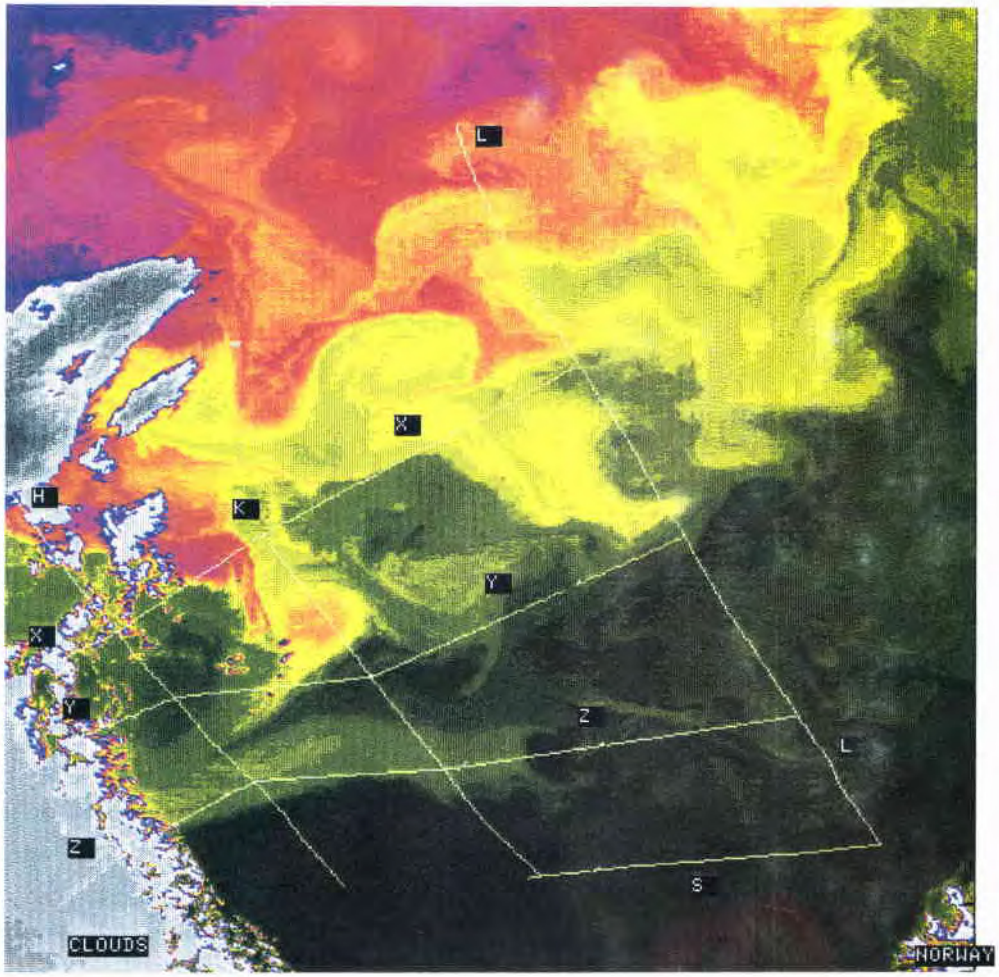

Figure 5 *An infrared image of the southern Norwegian Sea showing the variability of the sea-surface temperatures at ca. 11 μm wavelength (T_4), with blue representing cold water and red warm water. The data are from the AVHRR/2 on the NOAA-7 spacecraft on 16 November 1984 at 14:54 UTC. The cloud-free parts of the sections shown were used. The letters serve to identify the sections in subsequent figures and tables. This is the winter, daytime image.*

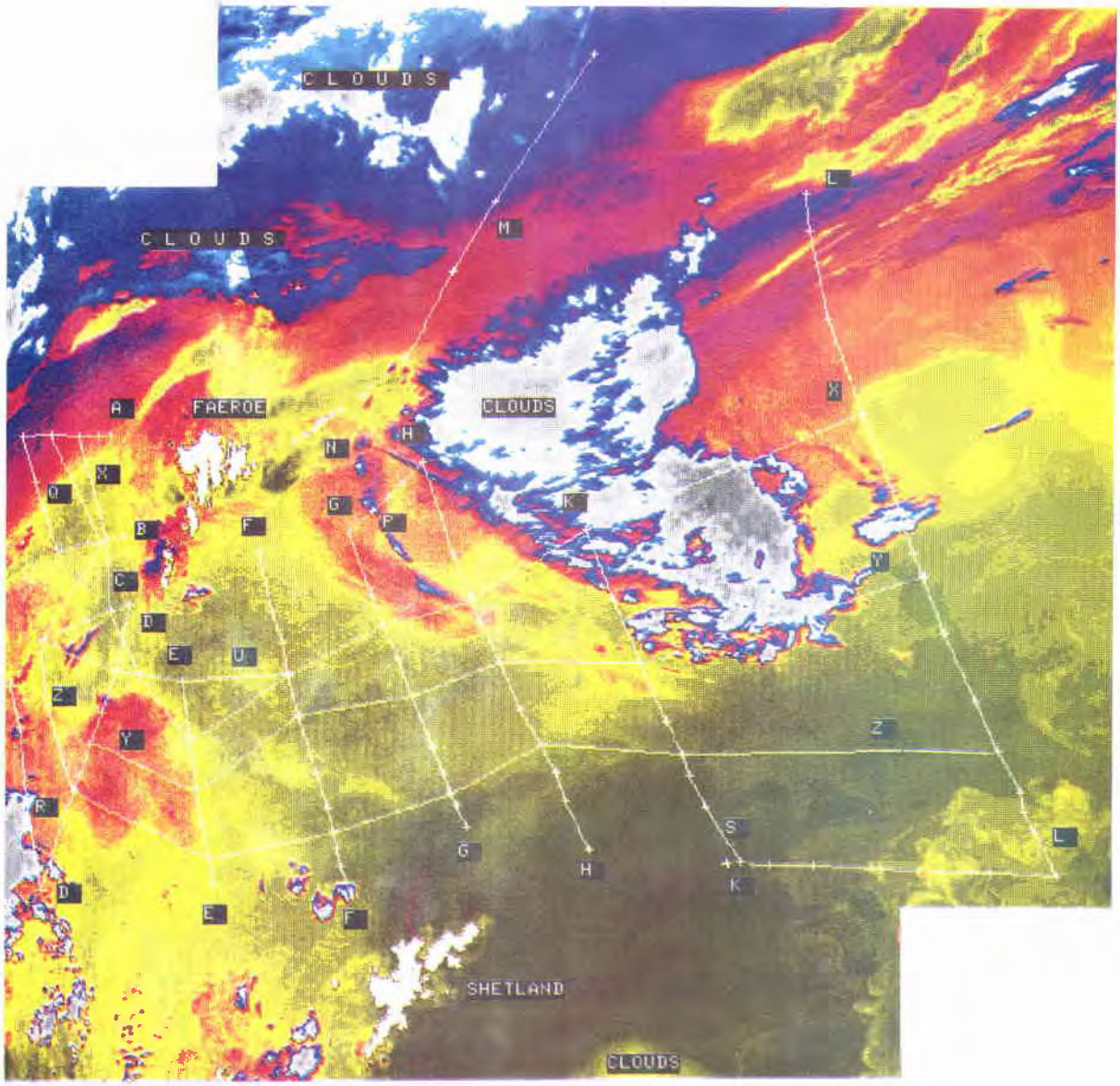

Figure 6 *An infrared image of the southern Norwegian Sea showing the variability of the sea-surface temperatures at ca. 11 μm wavelength (T_4), with blue representing cold water and red warm water. The data are from the AVHRR/2 on the NOAA-9 spacecraft on 16 June 1986 at 13:04 UTC. The cloud-free parts of the sections shown were used. The letters serve to identify the sections in subsequent figures and tables. This is the summer, daytime image.*

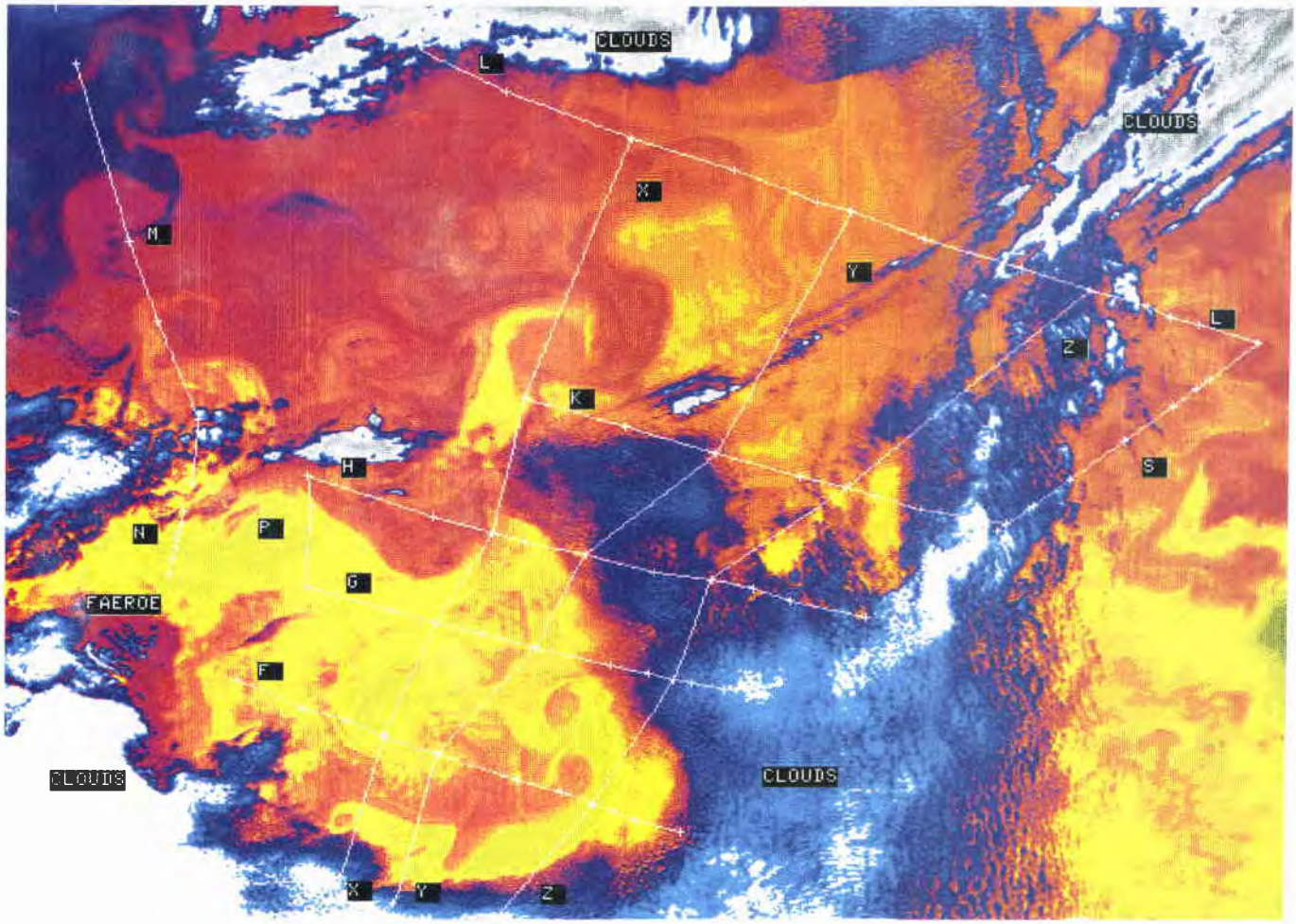

Figure 7 *An infrared image of the southern Norwegian Sea showing the variability of the sea-surface temperatures at ca. 11 μm wavelength (T_4), with blue representing cold water and red warm water. The data are from the AVHRR/2 on the NOAA-9 spacecraft on 21 June 1986 at 03:53 UTC. The cloud-free parts of the sections shown were used. The letters serve to identify the sections in subsequent figures and tables. This is the summer, night-time image.*

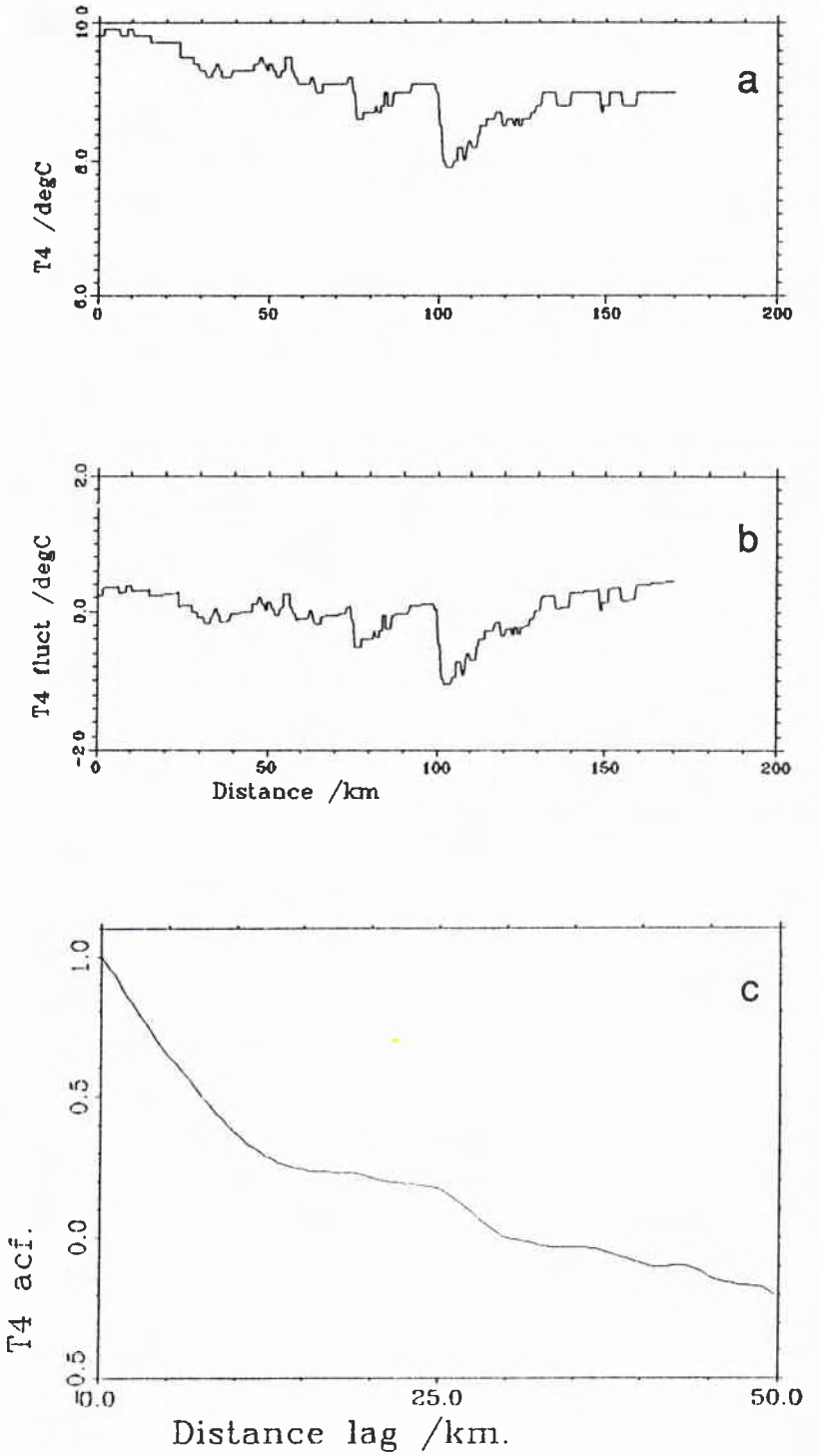

Figure 8 *Temperature section (a) extracted along the line S from the T_4 image of 16 June 1986 (see Fig. 6), (b) after the removal of a small linear trend, which is given in Table 6. The space-lagged autocorrelation function is shown in (c).*

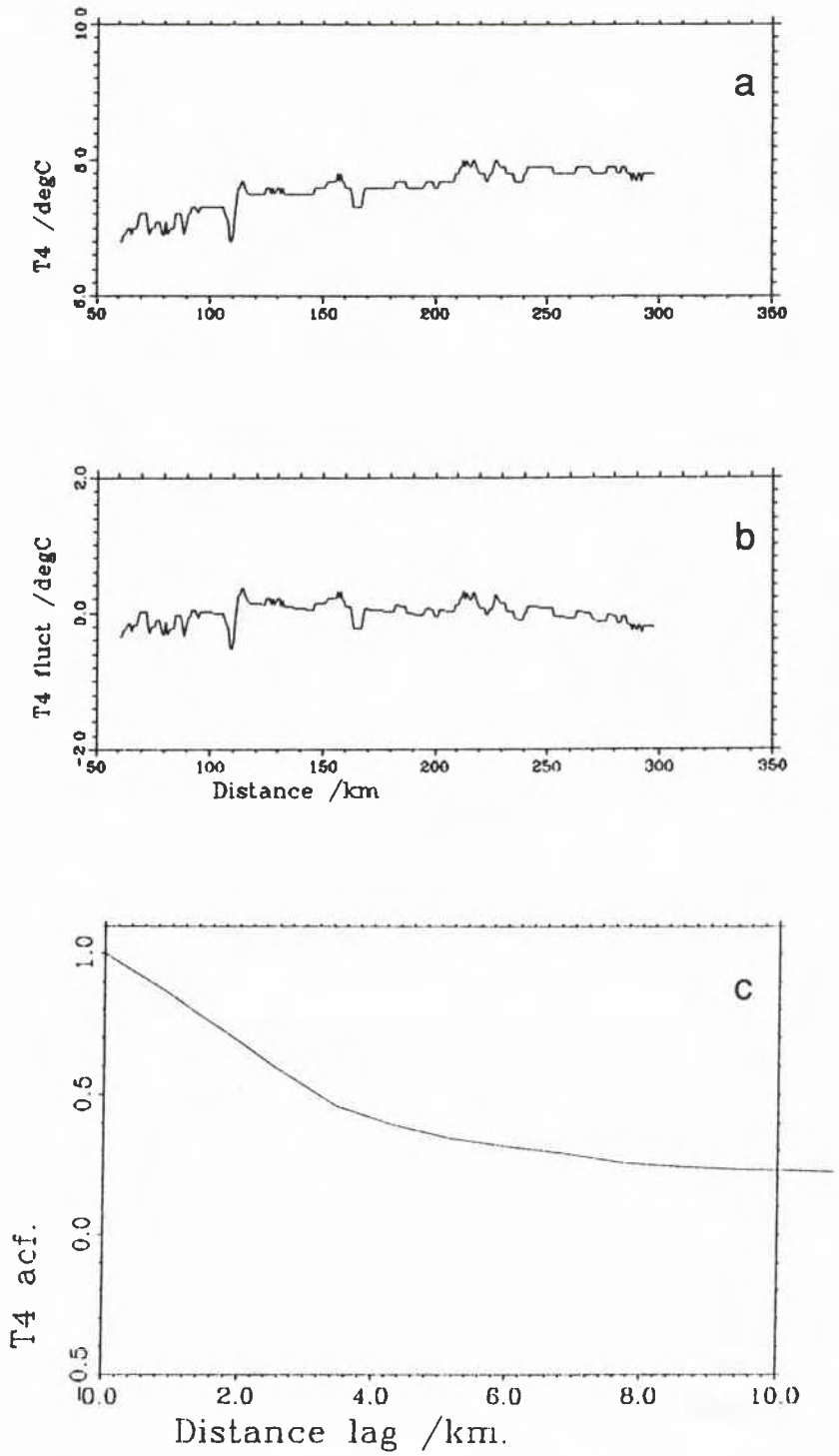

Figure 9 *Temperature section (a) extracted along the line L from the T_4 image of 21 June 1986 (see Fig. 7), (b) after the removal of a small linear trend, which is given in Table 6. The space-lagged autocorrelation function is shown in (c).*

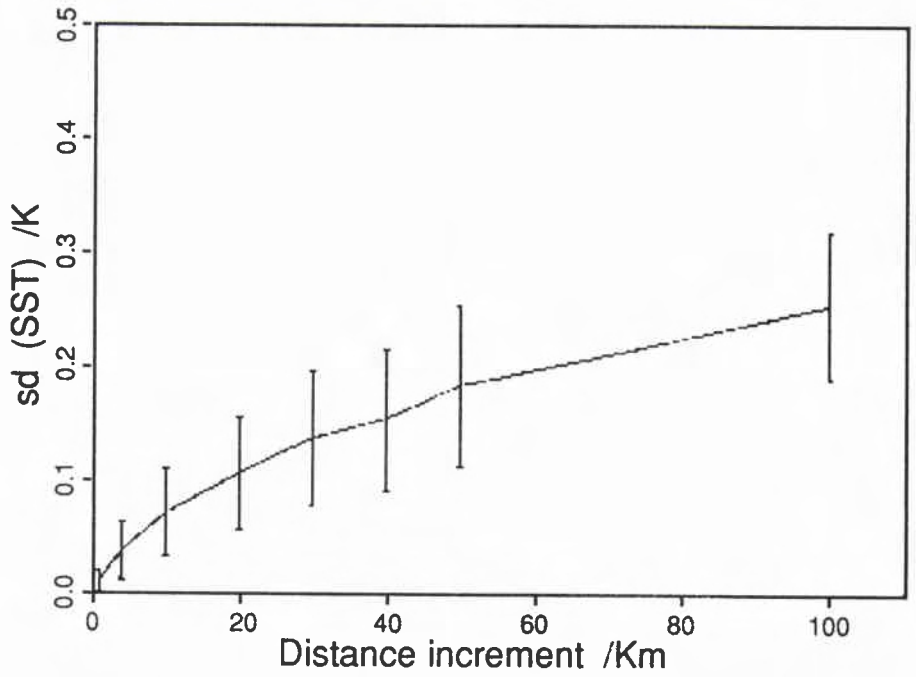

Figure 10 *SST variability as perceived from a transiting research ship. Some 22 days worth of 1-min data samples were divided into segments of fixed lengths and the standard deviation of SST in each segment was calculated. The line shows the mean, with bars representing one standard deviation, of the standard deviations for each segment length.*

4

Results and discussion

For the purposes of using in situ SST measurements to validate satellite data, the separation in time or space between two measurements that gives rise to an rms difference of 0.2 K is an appropriate quantity to determine. The following discussion (Subsect. 4.1) concentrates on the values of $\Delta_{0.2\,\mathrm{K}}$, which is the spatial separation, and $\tau_{0.2\,\mathrm{K}}$, which is the elapsed time interval, each of which would contribute ± 0.2 K to the error budget of the satellite validation. However, for the purposes of using SST measurements, from whatever source, with numerical ocean models in which the data assimilation scheme uses a weighting function related to the autocorrelation function (e.g. the optimum interpolation scheme of Gandin (1963)), then other quantities more directly related to the autocorrelation of the SST field may be more appropriate. For this reason the lags over which the a.c.f. decay to a value of 0.5, $\Delta_{1/2}$ and $\tau_{1/2}$, have also been derived and are discussed in Subsect. 4.2.

4.1. SATELLITE SST VALIDATION

Temporal variability The measurements of SST from the two ASID buoys can be used to characterise the temporal variability in this area. The a.c.f. values were calculated for the two time series to determine the size of $\tau_{0.2\,\mathrm{K}}$, the time interval separating two SST measurements that causes an rms difference of ± 0.2 K between them. The deterministic trend in the data is the seasonal heating cycle, which may be better approximated over the three month period of the time series by a quadratic rather than linear function. Consequently, the a.c.f. values were calculated for the residuals after removal of both linear and quadratic trends and the results are given in Table 2.

The measurements from Buoy 4125 have larger a variance of the fluctuations about a linear trend, but this is more than halved when a quadratic trend is removed, and this leads to a significant increase in $\tau_{0.2\,\mathrm{K}}$ to 19 h. This is not so for the data from Buoy 4126, in which case the variance of the fluctuations decreases by only $\sim 50\%$ and $\tau_{0.2\,\mathrm{K}}$ remains < 4 h. Examination of the temperature signals themselves shows the time series from Buoy 4126 to contain more sharp temperature changes than that from Buoy 4125, and these rapid changes cause the a.c.f. values to decay quickly at short lags. The larger temperature steps are indicative of the buoys passing through the surface outcrops of thermal fronts which puts into question the assumption that

the buoys are providing a true Lagrangian measurement. The surface float of these buoys is small, so that their passage through the water is unlikely to be a result of the wind alone; more likely it is the result of differential drag on the thermistor chain caused by current shear along its length.

The values of $\tau_{0.2\,K}$ calculated for each of the 10-day segments of the ASID buoy SST measurements are given in Tables 3a and b. The a.c.f. values were calculated for these relatively short segments only for the residuals remaining after the removal of linear trends. For Buoys 4125 the values of $\tau_{0.2\,K}$ are much longer and more variable (mean $\pm$ 1 standard deviation being 7.5 h $\pm$ 4.6 h) than those of Buoy 4126 (1.7 h $\pm$ 0.5 h). Indeed, for the first segment of data from Buoy 4125 (which is somewhat shorter than the 10-day interval of all other segments because of the later deployment of this buoy), the residual SST fluctuations are so small that $\tau_{0.2\,K}$ is undefined. The results from Buoy 4126 imply that an elapsed time of several hours between an in situ measurement and the corresponding satellite overpass could be tolerated during a validation exercise, whereas those from Buoy 4125 imply a maximum of 2 h, and preferably shorter. The discrepancies between the $\tau_{0.2\,K}$ values from the two buoys is rather disquieting. Indeed, closer inspection of the time series shows the Buoy 4125 SST time series to resemble more the character of the near-surface thermistor-chain time series than is the case for Buoy 4126. Both time series were subjected to the same data processing scheme, so there remains only the uncertainty that the two SST thermistors had a systematic difference. Perhaps Buoy 4125 was floating deeper in the water and therefore measured at a greater depth, or perhaps Buoy 4126 was floating too high in the water, or not vertically, so that the level of the SST thermistor was frequently exposed above the water level thereby introducing a spurious higher frequency signal. At this point there is no means of testing either of these hypotheses.

To err on the side of caution, the results of Buoy 4126 should be seen as correct, and in situ measurements and satellite data separated by more than 2 h should not be used for satellite data validation.

Spatial variability The values of $\Delta_{0.2\,K}$ calculated for each section extracted from the three AVHRR images are given in Tables 5–7 and their distribution are summarised in Table 8. Most values ($\sim$ 80%) of $\Delta_{0.2\,K}$ are $<$ 20 km and the majority ($\sim$ 60%) are $<$ 10 km. However, some are significantly longer than 20 km. A few sections on the order 100 km are such that the standard deviation of the SST is $<$ 0.2 K, and in these cases a sample SST measurement is valid, at least at the level of $\pm$0.2 K, over a large area. To be useful for satellite validation, such areas would need to be sought out as they are constitute only $\sim$ 10% of the cases studied here. The general case in which $\Delta_{0.2\,K} \leq$ 10 km implies very little margin in the collocation of the satellite and in situ data, as at least half of this distance can be accounted for in uncertainties in locating a given geographical point in the satellite image. The corresponding uncertainty in the position of the in situ measurement is much smaller, being $<$ 1 km for ARGOS buoys (Miller et al., 1989) and better for

research vessels using satellite navigation. Nevertheless, the permitted discrepancy between the satellite and in situ measurements is only a few pixels.

Table 8 *Distributions of* $\Delta_{0.2\,\mathrm{K}}$ *and* $\Delta_{1/2}$

Lag (km)	Environmental conditions			
	Winter	Summer		Total
	day	day	night	
Autocorrelation function lag $= \Delta_{0.2\,\mathrm{K}}$ *				
≤ 5	5	4	5	14
≤ 10	8	6	9	23
≤ 20	8	11	10	29
> 20	2	5	0	7
Autocorrelation function lag $= \Delta_{1/2}$ **				
≤ 5	1	5	6	12
≤ 10	4	11	10	25
≤ 20	9	14	10	33
> 20	1	2	0	3

* Autocorrelation function has a value corresponding to rms differences of ± 0.2 K between samples separated by $\Delta_{0.2\,\mathrm{K}}$ km.
** Autocorrelation function has a value of 0.5.

The variations of $\Delta_{0.2\,\mathrm{K}}$ from image to image is shown in Table 9. The presence of clouds over the area in the summer night-time image and the winter image reduces considerably the number of comparisons of individual sections that can be made. There is slight evidence that $\Delta_{0.2\,\mathrm{K}}$ is smaller at night (7.6 km in the mean compared with 13.0 km during the day) when the nocturnal heat loss augments any wind-mixing in the surface layer; even though there is a slight decrease in the SST variance (mean standard deviation of T_4 being 0.29 K), the increased level of mixing may be contributing to a reduction in the scales of the variability. During the winter, with the erosion of the seasonal thermocline, the SST patterns are coupled to thermal structures extending deeper into the water column. The observed SST variance is somewhat greater in the winter (standard deviation of T_4 is 0.46 K in the mean), and the scales of $\Delta_{0.2\,\mathrm{K}}$ are also shorter (7.5 km in the mean), again possibly indicating higher levels of mixing activity. The small number of cases examined here naturally dictates caution in the interpretation of any seasonal or diurnal effects as these differences may not be significant.

Also shown in Table 9 is the orientation of the section relative to the inflowing Norwegian Atlantic Current, but there is no evidence of a dependence of $\Delta_{0.2\,\mathrm{K}}$ on the along-stream or cross-stream direction. Instead, the spatial distribution of

$\Delta_{0.2\,K}$ (Fig. 11) shows it to localise in areas of high or low values irrespective of the orientations of the sections relative to the stream, indicating the areas of short $\Delta_{0.2\,K}$ being associated with areas of high mesoscale variability that are not noticeably anisotropic. This is confirmed by inspection of the satellite images themselves, which show that the areas of large horizontal temperature gradients are swept up into eddies, thereby losing any dominant orientation with respect to the stream.

Table 9 *Variation of $\Delta_{0.2\,K}$, the lag for which the rms difference is ±0.2 K (all distances are in km)**

Sect.	Orientation[1]	Summer		Winter
		day	night	day
A	X	–		
B	X	–		
C	X	1.6		
D	X	4.8		
E	X	34		
F	X	27	6.8	
G	X	15	15	
H	X	14	2.0	3.3
K	X			4.3
L	X	16	22	3.7
M	X	2.6	3.1	
S	A	2.4	3.3	7.7
U	A	8.8		
X	A	9.2	7.2, 9.3	4.6, 2.4
Y	A	15	6.5, 0.8	–, 6.6
Z	A	18		29, 5.8

* Dashed lines indicate that the value of $R(\Delta_{0.2\,K})$ is not encountered.

[1] X denotes section aligned across the mean surface flow; A denotes section aligned along the mean surface flow.

In all the examples discussed here, a linear least-squares trend was removed from the section before calculating the autocorrelation functions. This was to avoid the domination of the autocorrelation functions by a large scale trend which may be deterministic in nature. In such a case, the trend, determined by a large scale survey of the area or from climatology, should then be taken into account in the procedure comparing satellite data with in situ data at a distance. In reality, the trends are so small (Tables 5–7) and the distances $\Delta_{0.2\,K}$ are so short that the consideration of the larger scale SST trends is irrelevant in most cases.

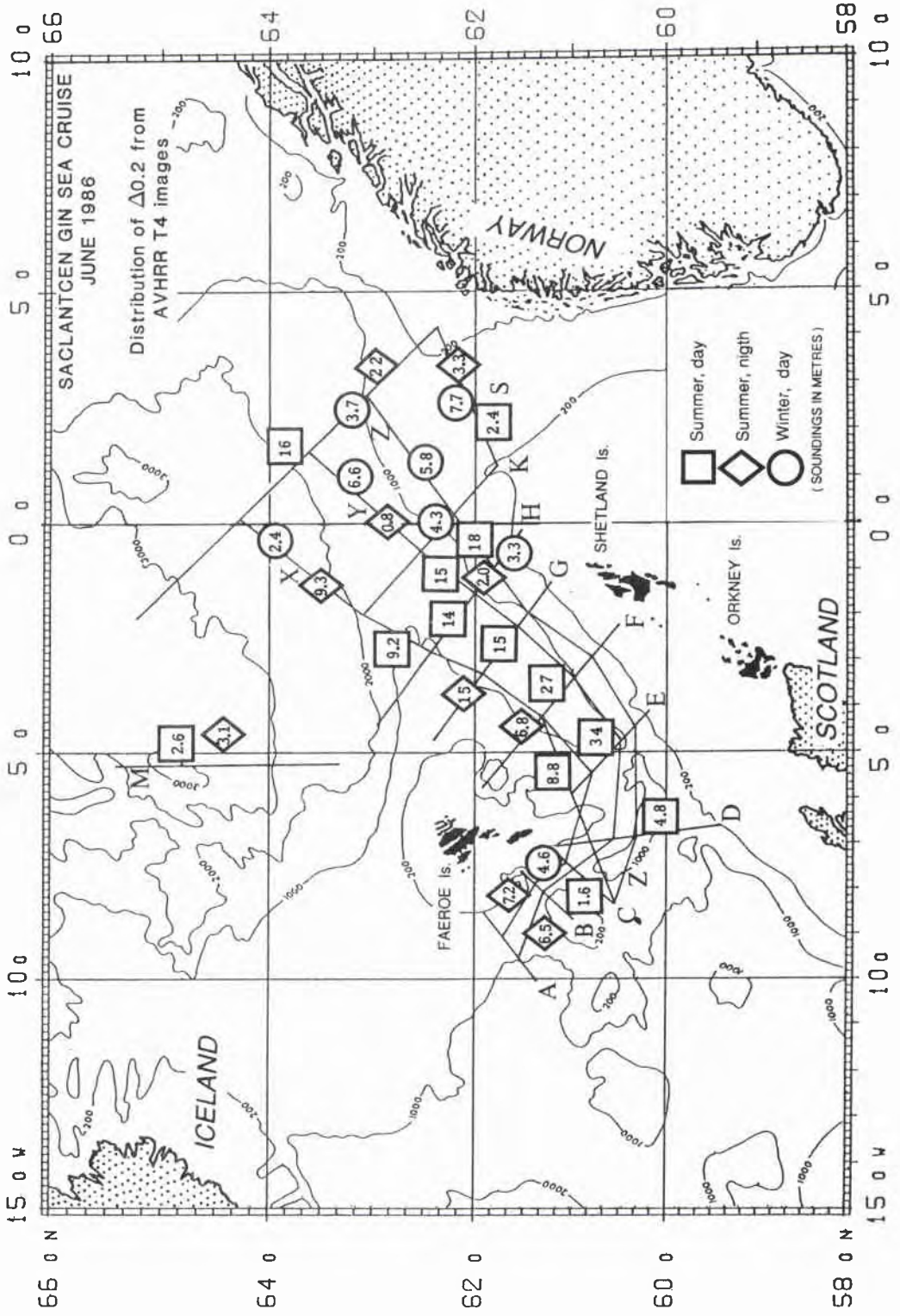

Figure 11 *The spatial distribution of $\Delta_{0.2\,K}$, the lag at which the space-lagged autocorrelation function has decayed to a value corresponding to an rms difference of ca. 0.2 K between pairs of measurements separated by $\Delta_{0.2\,K}$ km. The numbers are those listed in Table 9.*

Variability in ship-borne SST time series The results the analysis of the SST measurements from the research ship *Tydeman* are shown in Fig. 10. At first sight it would appear that, in the mean, the segment length corresponding to a standard deviation of ± 0.2 K, $\sim$ 60 km, is significantly longer than the maximum tolerable separation derived from the $\Delta_{0.2\,\mathrm{K}}$ values. However, the mean case may be inappropriate as the distribution of the standard deviations of SST within each segment length is very broad, as is shown by the bars in Fig. 10. A more prudent interpretation of these results may be to consider the segment length for which the mean plus one standard deviation, or the mean plus two standard deviations, falls below the 0.2 K level, in which case the acceptable segment length becomes $\sim$ 30 km or $\sim$ 15 km, which approaches the $\Delta_{0.2\,\mathrm{K}}$ value. The difference between this result and that derived from the AVHRR data should not come as a surprise since two different quantities are involved, each being derived from a different data source. Also, by definition, the acceptable separation derived from the $\Delta_{0.2\,\mathrm{K}}$ data should be shorter than that derived from the SST variances in segments of various lengths. However, perhaps implicit in this result is the effect of detector noise in the AVHRR data, which is introducing high frequency fluctuations that cause an accelerated decay of the autocorrelation function and thence an estimate of $\Delta_{0.2\,\mathrm{K}}$ that is too small. Nevertheless, the shorter estimate of the tolerable separation, $\sim$ 10 km, should still be adopted, even if only to err on the side of caution.

4.2. DATA ASSIMILATION IN OCEAN MODELS

Temporal variability For the time series of the ASID buoy temperature measurements considered as a whole, the values of $\tau_{1/2}$ are long for fluctuations about the linear trend (Table 2), but are about halved for the more physically meaningful fluctuations about a quadratic trend. For the 10-day sections the values of $\tau_{1/2}$ are further reduced, being in the mean 12.3 $\pm$ 7.4 h for Buoy 4125 and 5.3 $\pm$ 4.2 h for Buoy 4126 (the large standard deviations are the result of a few big values of $\tau_{1/2}$ that also bias the mean value), and have median values of 9 h for Buoy 4125 and 4 h for Buoy 4126.

The time steps of upper ocean circulation models are generally of the same order as the median $\tau_{1/2}$ values, i.e. several hours. This implies that SST values, either satellite-derived or from in situ measurements, are of some value irrespective of the time interval between the observations and the model time step. This conclusion is valid only in areas where the temporal changes are not dominated by the advection of horizontal temperature gradients. In such cases no statements can be made without knowledge of the surface current characteristics and SST gradients other than that measurements taken closest in time to the model time step are of most value.

Spatial variability The distribution of the values of $\Delta_{1/2}$ is quite similar to that of $\Delta_{0.2\,K}$ with $\sim$ 90% of all being < 20 km (Table 7), i.e. corresponding to ca. $\leq 0.2°$ latitude. This implies that measurements, either in situ or from a satellite, taken more than 20 km from a grid point are of little use as the rms difference between them and the values of the field at the positions of the grid points would be greater than the standard deviation of the fluctuations of the SST field. There appears to be no significant seasonal change in the mean value of $\Delta_{1/2}$ (Table 10), in that it is 10.4 km in June and 11.6 km in November. It is halved for the June night-time example (5.2 km) but it is not clear that this is a significant result given the small sample size. As with $\Delta_{0.2\,K}$, there is no strong dependence on the orientation of the section with respect to the mean surface current.

Table 10 *Variation of $\Delta_{1/2}$, the lag at which autocorrelation function has decayed to a value of 0.5 (all distances are in km)*

Sect.	Orientation[1]	Summer		Winter
		day	night	day
A	X	5.0		
B	X	3.5		
C	X	2.7		
D	X	2.7, 3.2		
E	X	6.6		
F	X	7.9	9.4	
G	X	11	5.0	
H	X	8.4	4.4	15
K	X			14
L	X	20	3.2	8.1
M	X	7.5	6.1	
S	A	7.5	2.9	8.2
U	A	9.2		
X	A	15	10, 4.9	25, 12
Y	A	31	5.5, 2.4	4.2, 12
Z	A	25		6.3, 11

[1] X denotes section aligned across the mean surface flow; A denotes section aligned along the mean surface flow.

5

Summary and conclusions

Sea-surface temperature measurements from various sources have been analysed to characterise the variability of the SST fields, both spatial and temporal, as well as the way that it is perceived from a moving research ship, to ascertain the differences caused by lack of collocation and simultaneity between two measurements. The purpose of this is to attempt to specify acceptable limits on the lack of precise coincidence between an in situ measurement that is intended to be used for the validation of satellite SST retrievals, and the nearest satellite measurement. Similarly, the inherent variability of the SST field has a consequence on the utility of SST measurements for initialising, updating or verifying numerical upper ocean models when the real SST data do not lie at the positions of the model grid points.

The spatial variability has been described from temperature sections extracted from infrared images of the AVHRR, while the temporal variability has been explored using SST measurements from free-drifting meteorological buoys. The satellite data are a very good approximation to a synoptic data set, but there is evidence in the buoy data of changes due to advection of the buoy through horizontal temperature structure, so that the description of the temporal evolution of SST is less than ideal. The SST variability as perceived from a research vessel transiting between oceanographic stations has also been examined. All data are from the area of the southern Norwegian Sea in the Norwegian Atlantic Current, and the SST variability resulting from the presence of fronts and eddies of moderate strength, but interspersed with areas of smaller gradients, may be considered to be reasonably representative of much of the world's oceans.

For the purposes of satellite data validation, a discrepancy of up to 0.2 K between the satellite and the in situ data may be tolerated. The results presented here show that time differences of up to two hours and spatial displacements of up to 10km may be acceptable, or a similar distance along the track of a ship that is travelling at $\sim$ 10 kn. There is slight evidence that the acceptable spatial displacements are shorter at night and during the winter, but the number of cases studied is too small to confidently conclude that satellite validation is best carried out in the summer months during daylight, although from totally independent considerations, those of being able to use scattered sunlight at visible or near-infrared wavelengths to detect clouds, daytime data are generally more reliable. At the small scales involved here, there is no strong evidence of spatial anisotropy in the SST variability, although this is apparent at scales of 50 km and more (Viehoff, 1989). The constraints presented here are more stringent than those concluded from earlier preliminary results (Minnett, 1989).

Although the acceptable displacements are in general very small, and in practice should be reduced yet further to allow for uncertainties in the geolocation of the satellite measurements, there are situations where the SST variability is so small that the standard deviations of temperature sections of 100 km and more are less than ± 0.2 K. It would seem advisable to seek out, wherever possible, such areas for satellite data validation exercises. It is likely, however, that these locations are not stationary or readily identified well in advance of a validation campaign, as they are associated with the absence of fronts at current and eddy boundaries which are themselves transient.

It is tempting to assign part of the apparent improvement in the accuracy of AVHRR SST retrievals over recent years to the increasingly narrow windows of elapsed time and spatial discrepancies between the satellite data and the corresponding in situ measurements. For example, Strong and McClain (1984) accepting drift buoy data within 24 h and 50 km of satellite data deduced an rms difference of 0.68K attributed to the satellite measurements; Llewellyn-Jones et al. (1984) accepted research vessel data within 2.5 h and used mean values of cloud-free pixels from 50×50 pixel array ($\sim 41 \times 55$ km to $\sim 130 \times 56$ km) centred on the ship position and obtained an accuracy of 0.59 K; and recently Dalu and Liberti (1988) applied very strict limits (± 2 h and 0 km, and rejected measurements taken on days when there was evidence of the formation of a diurnal thermocline) and obtained accuracies of $\sim \pm 0.3$ K.

The penalty of stricter limits is fewer data points, and the consequence that a particular retrieval algorithm may not be validated over a broad enough range of conditions, or even in a statistically relevant fashion in a narrow range of conditions. It must be concluded, however, that a significant portion of the discrepancies between satellite and in situ data that is in the published literature is due to the variability of the SST field itself; it would appear that, in reality, the SST fields derived from AVHRR measurements could be a good deal more accurate than is currently demonstrated on the strength of comparisons with in situ data.

Given the extreme logistical difficulties in obtaining high quality in situ measurements for direct validation of satellite SST validation, it may be worth considering a complementary method, that of using a low-flying aircraft to measure SST in cloud-free areas or an aircraft to measure the upwelling radiance from the sea surface at various heights through the atmosphere (Hagan, 1988; Minnett and Saunders, 1989), thereby validating the radiative transfer models used to derive the satellite SST retrieval algorithms by simulating the satellite radiometer measurements (e.g. Llewellyn-Jones et al. 1984; Minnett 1986, 1988, 1990b).

For the use of SST data, derived either from satellites or in situ measurements, in ocean models, the constraints on spatial displacement of an SST measurement from a model grid point or the elapsed time from a model time step are slightly less severe than for satellite validation. However, the SST measurement contains no useful information at displacements of more than ~ 20 km and at time intervals of

more than $\sim$ 6 h. Given that the time steps of upper-ocean models are generally much less than 6 h, the time at which measurements are made appears to be largely immaterial. But the spatial constraint is significant. The situation is more complex if it is considered that a grid-point value represents a mean over a large area, an aspect that is not considered here. Nevertheless, given that model grid points are typically 50–100 km apart at best, it must be concluded that many SST measurements (and also estimates of air-sea fluxes, the scales of which are dependent on those of SST) are decorrelated from the values at the nearest grid point and therefore do not contribute significant information to the model simulations.

The results presented here are restricted to the temperature of the sea surface and should be applied to deeper temperature structure only with the greatest caution. There is evidence that temperature variability has longer time scales in the seasonal thermocline than at the surface (Viehoff and Fischer, 1988). However, in the vicinity of even quite weak fronts, very sharp spatial temperature changes may still occur (Minnett et al., 1983), and extremely complex horizontal temperature variability has been observed in high resolution thermistor chain transects of the Iceland-Faeroe Front (Scott, 1988, 1989). The temporal variability of subsurface temperature in the Norwegian Atlantic Current and elsewhere in the GIN Sea area is the subject of a separate study (Minnett and Hopkins, 1991).

References

Barton, I.J., Zavody, A.M., O'Brien, D.M., Cutten, D.R., Saunders, R.W. and Llewellyn-Jones, D.T. Theoretical algorithms for satellite derived sea-surface temperature. *Journal of Geophysical Research*, **94**, 1989: 3365–3375.

Bernstein, R.L. Sea surface temperature estimation using the NOAA-6 satellite Advanced Very High Resolution Radiometer. *Journal of Geophysical Research*, **87**, 1982: 9455–9465.

Brown, O.B., Brown, J.W. and Evans, R.H. Calibration of Advanced Very High Resolution Radiometer infrared observations. *Journal of Geophysical Research*, **90**, 1985: 11667–11678.

Castagne, N., Le Borgne, P., Le Vourch, J. and Olry, J.-P. Operational measurements of sea surface temperatures at CMS Lannion from NOAA-7 AVHRR data. *International Journal of Remote Sensing*, **7**, 1986: 953–984.

Cornillon, P. and Stramma, L. The distribution of diurnal sea surface warming events in the Western Sargasso Sea. *Journal of Geophysical Research*, **90**, 1985: 11811–11815.

Dalu, G. and Liberti, G.L. Validation problems for remotely sensed sea-surface temperature. *Il Nuovo Cimento*, **11**, 1988: 589–607.

Gandin, L.S. Objective Analysis of Meteorological Fields. Jerusalem, Israel Program for Scientific Translations, 1963.

Hagan, D.E. The profile of upwelling 11-m radiance through the atmospheric boundary layer overlying the ocean. *Journal of Geophysical Research*, **93**, 1988: 5294–5302.

Harries, J.E., Llewellyn-Jones, D.T., Minnett, P.J., Saunders, R.W. and Zavody, A.M. Observations of sea-surface temperature for climate research. *Philosophical Transactions of the Royal Society, London*, **309**, 1984: 381–395.

Hepplewhite, C.L. Remote observation of the sea surface and atmosphere: the oceanic skin effect. *International Journal of Remote Sensing*, **10**, 1989: 801–810.

Hopkins, T.S. Atlantic Inflow Experiment, GIN Sea cruise'86. Data Report Part 1: Hydrography, SACLANTCEN SM-209. La Spezia, Italy, SACLANT Undersea Research Centre, 1988.

Le Borgne, P., Le Vourch, J. and Marsouin, A. Sea surface parameters inferred from meteorological satellite data at CMS, Lannion. *International Journal of Remote Sensing*, **9**, 1988: 1819–1834.

Llewellyn-Jones, D.T., Minnett, P.J., Saunders, R.W. and Zavody, A.M. Satellite multichannel infrared measurements of sea-surface temperature of the N.E. Atlantic Ocean using AVHRR/2. *Quarterly Journal of the Royal Meteorological Society*, **110**, 1984: 613–631.

McClain, E.P. Global sea surface temperatures and cloud clearing for aerosol optical depth estimates. *International Journal of Remote Sensing*, **10**, 1989: 763–769.

McClain, E.P., Pichel, W.A., Walton, C.C., Ahmad, Z. and Sutton, J. . Multi-channel improvements satellite derived global sea surface temperatures. *Advanced Space Research*, **2**, 1983: 43–47.

Miller, G.S., Muzzi, R.W., Dungan, J.E. and Saylor, J.H. . Adding LORAN-C position recording to a satellite-tracked drifter buoy. *Marine Technology Society Journal*, **23**, 1989: 36–38.

Minnett, P.J. A numerical study of the effects of anomalous North Atlantic atmospheric conditions on the infrared measurement of sea-surface temperature from space. *Journal of Geophysical Research*, **91**, 1986: 8509–8521.

Minnett, P.J. The numerical simulation of infrared satellite measurements over the Greenland-Iceland-Norwegian Sea. SACLANTCEN SR-137. La Spezia, Italy, SACLANT Undersea Research Centre, 1988. [AD A 198 653]

Minnett, P.J. On the in situ validation of AVHRR measurements of sea-surface temperature. Proceedings of Fourth European AVHRR Data Users Meeting. EUMETSAT, Darmstadt-Eberstadt, Federal Republic of Germany. EUM P 06, 1989: pp 209–214.

Minnett, P.J. Satellite Infrared Scanning Radiometers – AVHRR and ATSR/M. *In:* Vaughan, R.A. *ed.* Microwave Remote Sensing for Oceanographic and Marine Weather Forecast Models. Dordrecht, Kluwer, 1990a: pp. 141–163.

Minnett, P.J. The regional optimisation of infrared measurements of sea-surface temperatures from space. *Journal of Geophysical Research*, (in press), 1990b.

Minnett, P.J. and Hopkins, T.S. Aspects of oceanographic variability observed from thermistor chains on free-drifting buoys. *In:* Potter, J.R. and Warn-Varnas, A. *eds.* Ocean Variability and Acoustic Propagation, Dordrecht, Kluwer, 1991. (To be published)

Minnett, P.J., Llewellyn-Jones, D.T. and Zavody, A.M. Satellite measurements of sea-surface temperature for climate research. *In:* Gautier, C. and Fieux, M. *eds.* Large-scale Oceanographic Experiments and Satellites Dordrecht, Reidel, 1984: pp. 57–85.

Minnett, P.J., Pollard, R.T., Collins, D.S., Horch, A. and Knoll, M. The structure of a weak thermohaline front. *Philosophical Transactions of the Royal Society, London*, **308**, 1983: 359–375.

Minnett, P.J. and Saunders, R.W. Validation of spacebourne radiometers: co-ordinated ship and aircraft measurements. Proceedings of Fourth European AVHRR Data Users Meeting. EUMETSAT, Darmstadt-Eberstadt, Federal Republic of Germany. EUM P 06, 1989: 329–334.

Robinson, I.S., Wells, N.C. and Charnock, H. The sea surface thermal boundary layers and its relevance to the measurement of sea surface temperature by airborne and spaceborne radiometers. *International Journal of Remote Sensing*, **5**, 1984: 19–46.

Schluessel, P., Shin, H.-Y., Emery, W.J. and Grassl, H. Comparison of satellite-derived sea-surface temperature with in-situ skin measurements. *Journal of Geophysical Research*, **92**, 1987: 2859–2874.

Scott, J.C. IF '86 – An introductory analysis of the thermistor chain data set. ARE TM (UJO) 88131. Portland, UK, Admiralty Research Establishment, 1988.

Scott, J.C. IF '87 – An introduction to the thermistor chain data set. ARE TM (UJO) 89102. Portland, UK, Admiralty Research Establishment, 1989.

Sparkman, J.K. NOAA polar orbiting sensor systems: today and tomorrow. *International Journal of Remote Sensing*, **10**, 1989: 609–612.

United States National Aeronautics and Space Administration 1986. Moderate-Resolution Imaging Spectrometer (MODIS) Instrument Panel Report. Earth Observing System Reports volume IIb.

Viehoff, T. Mesoscale variability of sea surface temperature in the North Atlantic. *International Journal of Remote Sensing*, **10**, 1989: 771–785.

Viehoff, T. and Fischer, J. Satellite-SST at the North Atlantic Polar Front related to high resolution towed CTD-data. *Journal of Geophysical Research*, **93**, 1988: 15551–15560.

Walton, C. Satellite measurement of sea surface temperature in the presence of volcanic aerosols. *Journal of Climate and Applied Meteorology*, **24**, 1985: 501–507.

Webster, F. and Fieux, M. TOGA overview. *In:* Gautier, C. and Fieux, M. *eds.* Large-scale Oceanographic Experiments and Satellites, Dordrecht, Reidel, 1984: pp. 17–26.

Initial Distribution for SR-165

Ministries of Defence	
JSPHQ Belgium	2
DND Canada	10
CHOD Denmark	8
MOD France	8
MOD Germany	15
MOD Greece	11
MOD Italy	10
MOD Netherlands	12
CHOD Norway	10
MOD Portugal	5
MOD Spain	2
MOD Turkey	5
MOD UK	20
SECDEF US	60
NATO Authorities	
NAMILCOM	2
SACLANT	3
CINCIBERLANT	1
COMSUBACLANT	1
COMNAVSOUTH	1
SCNR for SACLANTCEN	
SCNR Belgium	1
SCNR Canada	1
SCNR Denmark	1
SCNR Germany	1
SCNR Greece	1
SCNR Italy	1
SCNR Netherlands	1
SCNR Norway	1
SCNR Portugal	1
SCNR Spain	1
SCNR Turkey	1
SCNR UK	1
SCNR US	2
French Delegate	1
SECGEN Rep. SCNR	1
NAMILCOM Rep. SCNR	1
National Liaison Officers	
NLO Canada	1
NLO Denmark	1
NLO Germany	1
NLO Italy	1
NLO Netherlands	1
NLO UK	1
NLO US	1
NLR to SACLANT	
NLR Belgium	1
NLR Canada	1
NLR Denmark	1
NLR Germany	1
NLR Greece	1
NLR Italy	1
NLR Netherlands	1
NLR Norway	1
NLR Portugal	1
NLR Turkey	1
NLR UK	1
Total external distribution	221
SACLANTCEN Library	10
Stock	29
Total number of copies	260